A spectroscopic study of southern (candidate) γ Doradus stars.

II. Detailed abundance analysis and fundamental parameters

H. Bruntt[1,2], P. De Cat[3,4], and C. Aerts[4,5]

[1] Niels Bohr Institute, University of Copenhagen, Juliane Maries Vej 30, DK-2100 Copenhagen Ø, Denmark
[2] School of Physics A28, University of Sydney, 2006 NSW, Australia e-mail: `bruntt@physics.usyd.edu.au`
[3] Royal Observatory of Belgium, Ringlaan 3, B-1180 Brussel, Belgium e-mail: `peter@oma.be`
[4] Katholieke Universiteit Leuven, Celestijnenlaan 200B, B-3001 Leuven, Belgium e-mail: `conny@ster.kuleuven.ac.be`
[5] Department of Astrophysics, Radboud University Nijmegen, 6500 GL Nijmegen, the Netherlands

ABSTRACT

Context. The γ Doradus stars are a recent class of variable main sequence F-type stars located on the red edge of the Cepheid instability strip. They pulsate in gravity modes, and this makes them particularly interesting for detailed asteroseismic analysis, which can provide fundamental knowledge of properties near the convective cores of intermediate-mass main sequence stars.
Aims. To improve current understanding of γ Dor stars through theoretical modelling, additional constraints are needed. Our aim is to estimate the fundamental atmospheric parameters and determine the chemical composition of these stars. Detailed analyses of single stars have previously suggested links to Am and λ Boo stars, so we wish to explore this interesting connection between chemical peculiarity and pulsation.
Methods. We have analysed a sample of γ Dor stars for the first time, including nine bona fide and three candidate members of the class. We determined the fundamental atmospheric parameters and compared the abundance pattern with other A-type stars. We used the semi-automatic software package VWA for the analysis. This code relies on the calculation of synthetic spectra and thus takes line-blending into account. This is important because of the fast rotation in some of the sample stars, and we made a thorough analysis of how VWA performs when increasing $v \sin i$. We obtained good results in agreement with previously derived fundamental parameters and abundances in a few selected reference stars with properties similar to the γ Dor stars.
Results. We find that the abundance pattern in the γ Dor stars is not distinct from the constant A- and F-type stars we analysed.

Key words. stars: fundamental parameters

1. Introduction

The members of the γ Dor class of variable stars are found near the main sequence on the cool edge of the Cepheid instability strip with spectral types A7–F5. They thus share properties with δ Scuti star variables, but the γ Dor periods are an order of magnitude longer, indicative of g mode pulsation. The γ Dor phenomenon was first identified by Balona et al. (1994), and Krisciunas & Handler (1995) presented the first list of six candidates. Henry et al. (2007) presents a list of 66 γ Dor stars, and the group continues to grow as new members are discovered both among field stars (Mathias et al. 2004; Henry & Fekel 2005; De Cat et al. 2006) and in open clusters (Arentoft et al. 2007). Only a few stars show pulsations characteristic of γ Dor and δ Scuti stars simultaneously (Henry & Fekel 2005; Rowe et al. 2006; King et al. 2007).

The γ Dor stars have given new hope for a deeper understanding of main sequence stars with masses around $2 M_\odot$ through asteroseismic analyses. Several δ Scuti stars have been studied extensively through both photometry and spectroscopy, and dozens of individual modes are now known in a few field stars (Breger et al. 2005) and also in members of open clusters (Bruntt et al. 2007). Whilst observational work has been very successful, comparison with theoretical models has so far not been able to provide a fully adequate description of all the ob-

servations (see Zima et al. 2006 for recent developments). While the driving in δ Scuti stars is well understood in terms of the opacity or κ mechanism, the link to predicting observed mode amplitudes is weak. Furthermore, theoretical models of δ Scuti stars show that even moderate rotation leads to significant shifts in the mode frequencies (Suárez et al. 2006b,a), which complicates the confrontation of observations and models.

The theoretical framework for interpreting the observed pulsation in γ Dor stars is well under way. Pulsations are thought to be driven by a flux blocking mechanism near the base of their convective envelopes (Dupret et al. 2004, 2006). Moya et al. (2005) investigated a method of constraining the models of γ Dor using frequency ratios. This method has been attempted on individual γ Dor stars (Moya et al. 2005; Rodríguez et al. 2006). While the method is indeed very useful for providing constraints, no unique models that fit all the observations were found. An improvement would be to better constrain the fundamental atmospheric parameters including metallicity. The star studied by Moya et al. (2005), HD 12901, is included in our sample.

In the current study we carry out a detailed abundance analysis of a sample of γ Dor stars described by (De Cat et al. 2006; hereafter Paper I) Thus, the current work is the second part of our detailed spectroscopic analysis of a sample of southern candidate γ Dor stars. In Paper I we made a detailed analysis of the spectra to study binarity and the pulsation properties. We identified 10 new bona fide γ Dor stars of which 40% are binary stars.

Table 1. Fundamental atmospheric parameters of the target stars as determined from photometric indices and parallaxes.

	Paper I		2MASS	Strömgren			HIPPARCOS
	Variability	$v \sin i$	$(V - K)$	$(b - y)$	m_1	c_1	π, T_{eff}, M & V
HD	type	[km s^{-1}]	T_{eff} [K]	T_{eff} [K]	[Fe/H]	$\log g$	$\log g$
7455	constant	3	**6400** ± 90	6070 ± 250	−0.17 ± 0.10	4.33 ± 0.20	**3.94** ± 0.20
12901	bf. γ Dor	64	**6950** ± 90	7200 ± 250	−0.33 ± 0.10	4.39 ± 0.20	**4.07** ± 0.13
14940	bf. γ Dor	39	**7090** ± 100	7200 ± 250	−0.23 ± 0.10	4.31 ± 0.20	**4.25** ± 0.12
22001	constant	13	**7130** ± 550	6690 ± 250	−0.07 ± 0.10	4.23 ± 0.20	**4.40** ± 0.19
26298	cand. γ Dor	50	**6780** ± 90	6730 ± 250	−0.36 ± 0.10	4.12 ± 0.20	**3.95** ± 0.21
27290	bf. γ Dor	54	**7310** ± 500	7200 ± 250	−0.01 ± 0.10	4.23 ± 0.20	**4.29** ± 0.18
27604	constant	70	**6320** ± 80	6450 ± 250	+0.09 ± 0.10	3.80 ± 0.20	**3.65** ± 0.11
33262	constant	14	**6060** ± 500	6130 ± 250	−0.21 ± 0.10	4.58 ± 0.20	**4.62** ± 0.20
40745	bf. γ Dor	37	**6900** ± 100	6950 ± 250	+0.08 ± 0.10	3.91 ± 0.20	**4.05** ± 0.12
48501	bf. γ Dor	40	**7240** ± 100	6980 ± 250	−0.12 ± 0.10	3.92 ± 0.20	**4.28** ± 0.12
65526	bf. γ Dor	53	**7170** ± 110	–	–	–	**4.40** ± 0.13
85964	constant	69	**6600** ± 90	6790 ± 250	−0.03 ± 0.10	4.09 ± 0.20	**4.14** ± 0.13
110379	cand. γ Dor	24	5450 ± 420	6860 ± 250	−0.17 ± 0.10	4.33 ± 0.20	4.39 ± 0.14
125081	bf. δ Scu	14	**6380** ± 90	6850 ± 250	+0.54 ± 0.10	3.69 ± 0.20	**3.44** ± 0.20
126516	cand. γ Dor	4	**6330** ± 90	6630 ± 250	−0.09 ± 0.10	4.37 ± 0.20	**4.17** ± 0.20
135825	bf. γ Dor	38	**7050** ± 90	7230 ± 250	−0.09 ± 0.10	4.30 ± 0.20	**4.39** ± 0.13
167858	bf. γ Dor	13	**7130** ± 100	7160 ± 250	−0.12 ± 0.10	4.14 ± 0.20	**4.23** ± 0.12
218225	bf. γ Dor	60	**6920** ± 100	–	–	–	**4.31** ± 0.21

Adopted values for the initial atmosphere models are printed in **bold**.

Detailed abundance analyses of γ Dor stars have only been done for a few individual stars. Bruntt et al. (2002) analysed the γ Dor star HD 49434 and found a metallicity slightly below solar, but the analysis was hampered by the high $v \sin i = 85$ km s^{-1}. Sadakane (2006) analysed HD 218396 and found solar abundance of C and O (but not S) and abundances of iron peak elements of −0.5 dex, thus suggesting a λ Boo nature for this star. Henry & Fekel (2005) found evidence that the γ Dor star HD 8801 is an Am star based on the strength of the Ca K line. Our aim is to shed light on these intriguing links that have been suggested between the γ Dor variables and the chemically peculiar λ Boo and Am-type stars (Gray & Kaye 1999; Sadakane 2006).

2. Observations and selection of targets

We have obtained high-resolution spectra with the échelle spectrograph CORALIE attached to the 1.2-m Euler telescope (La Silla, Chile) for a sample of 37 known and candidate γ Dor stars. For the details of the observations and the data reduction, we refer to Paper I. CORALIE covers the 3880–6810 Å region in 68 orders with a spectral resolution of 50 000. The typical S/N in the spectra is 100–150. For the abundance analysis, we selected the spectrum with the highest S/N. The wavelength calibrated spectra were rebinned to a step size of $\simeq 0.02$ Å. Each order was normalised by fitting low-order polynomials to continuum windows identified in a synthetic spectrum. The orders were then merged to a single spectrum while making sure the overlapping orders agreed.

Stars with projected rotational velocities $v \sin i > 70$ km s^{-1} have not been analysed due to two reasons: only very few unblended lines are available and we found that incorrect normalization of the spectra would introduce large systematic errors (Erspamer & North 2003). We also did not analyse the double-lined spectroscopic binaries from Paper I.

3. Aims and methods

The comparison of observed pulsation frequencies with theoretical models of γ Dor stars will provide important insight into main sequence stars with convective cores. It is important to constrain the model space by putting constraints on T_{eff}, $\log g$, and

metallicity from observations (Moya et al. 2005). Except for one star, our targets are single stars and their fundamental parameters must be estimated by indirect methods like the calibration of photometric indices and spectroscopic analysis. In the present analyses we rely on the former as input for a detailed abundance analysis, and we seek to improve the estimates of the fundamental parameters.

3.1. Realistic uncertainty estimates

The fundamental physical parameters of stars are mass, radius, and luminosity. These relate to the effective temperature, T_{eff}, and surface gravity, $\log g$. These two parameters, along with the metallicity, describe the properties of the applied model atmosphere in the abundance analysis. We adjust the parameters of the model to obtain a consistent result, specifically by requiring that the abundances measured for Fe lines of neutral and ionized species—and lines formed at different depths in the atmosphere—yield the same result. This is done by adjusting not only T_{eff}, $\log g$, but also the microturbulence (ξ_t), which is a crude parametrization of small-scale motions in the gas. We point out that in these analyses it is actually the temperature structure we adjust, but the final result we quote will be the T_{eff} and $\log g$ of the best-fitting model. It is thus not a direct measurement of the true values; therefore, it is important to assess how the fitted model parameters relate to the parameters of truly fundamental stars, i.e. stars where the properties are determined by model-independent means (Smalley 2005). The primary reference star is the Sun, but binary stars where accurate masses and radii have been determined are important for extending the validity of the method to higher temperatures. In our analysis we will test our method on the Sun and the visual binary HD 110379 (cf. Sect. 6).

Realistic uncertainties on T_{eff} and $\log g$ are especially important for our target stars, since some of them will likely be the targets for detailed asteroseismic studies. Our classical analysis of spectral lines yields intrinsic uncertainties on T_{eff} and $\log g$ in the range 50–100 K and 0.08–0.12 dex for slowly rotating stars. We estimate that at least 100 K and 0.1 dex must be added due to the limitations of the model atmosphere alone. This will lead
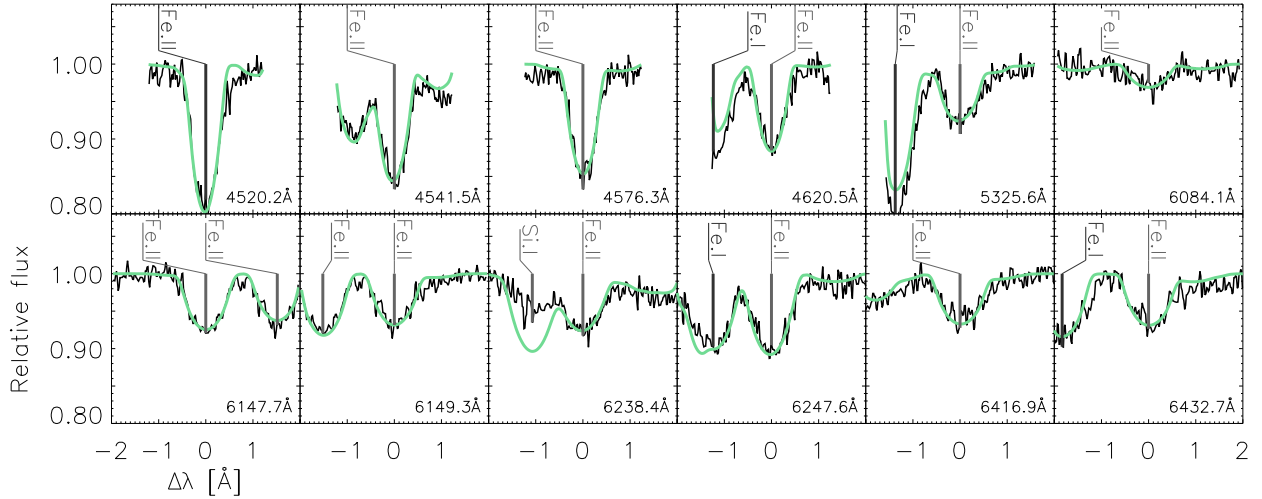
Fig. 1. Twelve Fe II lines in the candidate γ Dor star HD 110379 fitted by VWA (continuous line). The wavelengths of the fitted lines are given in the bottom right corner of each panel.

to uncertainties on the derived abundances of the order of 0.08 dex, which must be added to the measured intrinsic scatter.

3.2. Model atmospheres

We used model atmospheres interpolated in the fine grid published by Heiter et al. (2002). These models are based on the original ATLAS9 code by Kurucz (1993) but use a more advanced convection description (Kupka 1996) based on Canuto & Mazzitelli (1992). Our sample consists of A- and F-type stars that have shallow convection zones.

One of the physical assumptions in the models is local thermodynamical equilibrium (LTE), but deviations from LTE start to become important for the hotter stars. We have not included the NTLE corrections in the present analysis but will estimate the importance of the effect here. According to Rentzsch-Holm (1996), the correction for neutral iron is $[\text{Fe I/H}]_{\text{NLTE}} = [\text{Fe I/H}]_{\text{LTE}} + 0.1$ dex for stars with solar metallicity and $T_{\text{eff}} = 7300$ K. When this correction is applied, Fe II (unaffected by NLTE) must be increased by adding +0.2 to $\log g$. When extrapolating from Fig. 5 in Rentzsch-Holm (1996), the NTLE effect becomes negligible for stars cooler than about 6,000 K.

The initial model atmosphere used for the abundance analysis of each star has T_{eff} from the $V - K$ colour and $\log g$ from the HIPPARCOS estimates, except for HD 110379 where we used $\log g$ from the binary orbit (Smalley et al. 2002). For the metallicity we used the estimate from the Strömgren m_1 index and solar metallicity for the two stars that did not have this index (HD 65526 and HD 218225). We note that the photometric amplitudes in variable targets are so tiny that they will not affect the applied indices. We used an initial microturbulence of 1.5 km s^{-1} for all stars. The adopted values for the fundamental parameters used for the initial models are printed in bold face in Table 1.

4. Abundance analysis with VWA

The software package VWA (Bruntt et al. 2002, 2004) was used to measure abundances in the spectra and to constrain T_{eff} and $\log g$ for the slowly rotating stars. We have expanded VWA so it now has a graphical user interface (GUI), which allows the user

to investigate the spectra in detail, pick lines manually, inspect the quality of fitted lines, etc.

Abundance analysis with VWA relies on the calculation of synthetic spectra. We use the SYNTH code by Valenti & Piskunov (1996), which works with ATLAS9 models and atomic parameters and line-broadening coefficients from the VALD database (Kupka et al. 1999). Compared to classical abundance analyses based on equivalent widths, our analysis has two important advantages:

- The calculated spectrum includes contributions from neighbouring lines, and VWA can analyse stars with high $v \sin i$.
- Problems with normalization of the continuum can be recognized when comparing the observations with the calculated spectrum.

These effects gradually become stronger when going to shorter wavelengths.

In our experience when $v \sin i$ becomes larger than about 50 km s^{-1}, we cannot simultaneously constrain microturbulence, T_{eff}, or $\log g$. This is because increased line blending and improper normalization of the continuum will introduce relatively large systematic errors (Erspamer & North 2003; see also Sect. 6.4).

Each line is fitted by iteratively changing the abundance to match the equivalent width (EW) of the observed and calculated spectrum. The EW is computed in a wavelength interval equal to the full-width half-maximum (FWHM) of the line. In some cases, e.g. if the line is partially blended in one wing of the line, the range for fitting the EW must be changed manually in the GUI. On a modern computer (3.2 Ghz Pentium IV), it takes about one hour to fit 250 lines for a star with low $v \sin i$. The fitted lines are inspected in the GUI, problems with the continuum level or asymmetries in the line are readily identified, and these lines are discarded. This is done automatically by calculating the χ^2 of the fit in the core and the wings of the lines. This is followed by a manual inspection of the fitted lines.

An example of 12 lines fitted with VWA is shown in Fig. 1 for the star γ Dor candidate HD 110379. The star has a moderately high projected rotational velocity of $v \sin i \simeq 25 \text{ km s}^{-1}$. It is seen that a few of the lines are affected by blends from strong neighbouring lines. As an example of the line lists we have used,
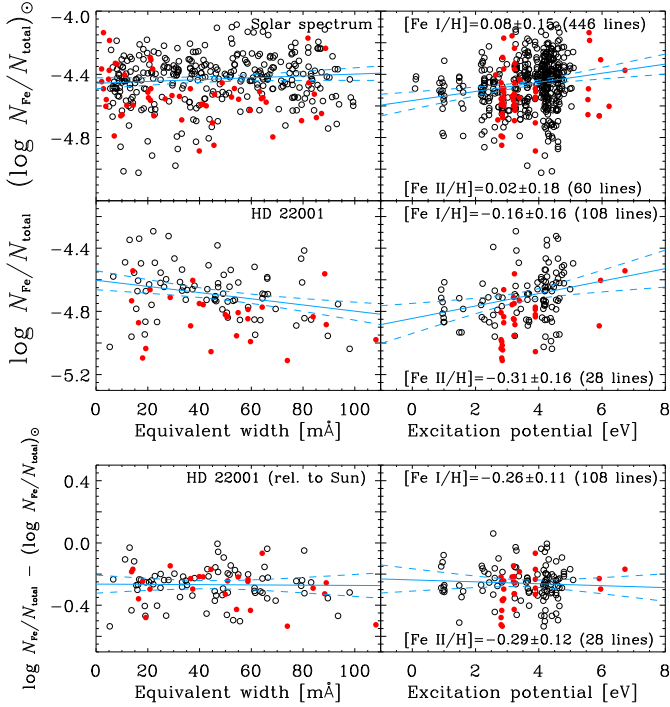
Fig. 2. The two *top panels* show the abundances of Fe in the reference spectrum of the Sun and the target star HD 22001. The open symbols are Fe I lines and solid symbols are Fe II lines. In the *bottom panel* the abundances in HD 22001 are measured relative to the same lines in the Sun. As a consequence the *rms* scatter decreases by 40%. The solid lines are linear fits and the dashed lines are 95% confidence limits.

we list the atomic parameters of the spectral lines we used for HD 110379 in Table B.1 in Appendix B.

4.1. Correcting log g values: relative abundances

In addition to the sample of stars in Table 1, we analysed a reference spectrum of the Sun (Hinkle et al. 2000), which has high resolution and high signal-to-noise (S/N ≃ 1, 000). Using the results for the solar spectrum allows us to make a more precise differential abundance analysis. The abundances of Fe I and Fe II lines measured in the Sun and HD 22001 are compared in the two *top panels* in Fig. 2. The abundances are plotted against equivalent width and excitation potential in the *left* and *right panels*, respectively. There are 446 Fe I lines in the Sun but only 108 lines are available for HD 22001, mainly because its spectrum has lower S/N and the star has higher $v \sin i$ (i.e. fewer unblended lines), and is about 1,200 K hotter than the Sun. The *rms* scatter of the Fe I abundance is about 0.15 dex for both stars.

It is seen that for the solar spectrum (*top panels* in Fig. 2), the abundance of Fe from neutral and ionized species do not agree and there is a significant positive correlation with excitation potential. The former could mean that log g is too high, while the latter indicates that the temperature of the model is too low. Since log g and $T_{\rm eff}$ are well-known for the Sun, we can make a first-order correction of the atmosphere models by measuring abundances in the target stars relative to the Sun. When doing this line-by-line any erroneous oscillator strengths, $\log gf$, are also corrected. This procedure has been used previously in detailed abundance studies of solar-like stars (Gonzalez 1998)
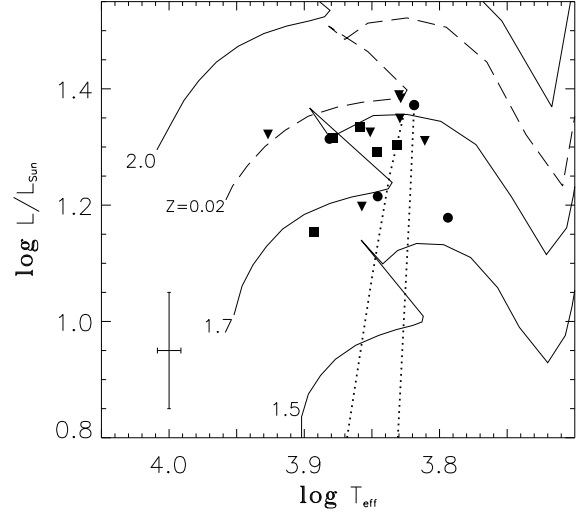

Fig. 3. Hertzsprung-Russell diagram for the sample of γ Dor candidate stars analysed. Circles, boxes, and triangle symbols are used for stars with low, moderate, and high $v \sin i$. Three evolution tracks from Lejeune & Schaerer (2001) are shown for metallicity $Z = 0.008$ (solid lines) and one track with $M/M_\odot = 2.0$ for Z=0.02 (dashed line). The dotted lines mark the γ Dor instability strip predicted from theoretical models by Dupret et al. (2005).

and also stars of earlier type (Gillon & Magain 2006). To give an idea of the magnitude of the log gf corrections, we quote the *rms* of the corrections for a few elements: C/Sc/Ni: 0.11 dex, O/Ca/Fe lines: 0.18 dex, S/Ti/Cr: 0.23 dex, and for Si: 0.46 dex.

The result of the differential abundance analysis for HD 22001 is shown in the *bottom panel* in Fig. 2. It is seen that the *rms* scatter in the Fe I and Fe II lines is lower by about 40%. While the differential analysis improves the internal precision of the measured abundances significantly, one should note that our targets are 300–1, 500 K hotter than the Sun, and therefore systematic errors could be the dominant source of uncertainty on the abundances and the fundamental parameters. The amount of convection will be quite different in the sample stars compared to the Sun, and the temperature structure in these model atmospheres may not describe the observed stars correctly (Heiter et al. 2002). The fact that the *rms* scatter decreases significantly gives us some confidence in the differential analysis, but systematic effects on $T_{\rm eff}$ or log g could be introduced. To explore this caveat, we analysed some secondary and tertiary reference stars that have spectral types similar to our targets.

4.2. New results for the abundance in the Sun

Based on time-dependent 3D hydrodynamical models, updated atomic line parameters, and NLTE corrections, Grevesse et al. (2007) recently revised the abundances in the Sun. The overall metallicity, Z, has decreased significantly from previous estimates (Grevesse & Sauval 1998), i.e. from 0.017 to 0.0122 (−30%), mainly due to the new C, N, and O abundances. This result has vast implications in many fields of astrophysics. This includes detailed asteroseismology of γ Dor stars, which the current work will provide important input to in terms of fundamental parameters and abundances. Our analysis was initiated before the new results, so they rely on the previous solar abundances
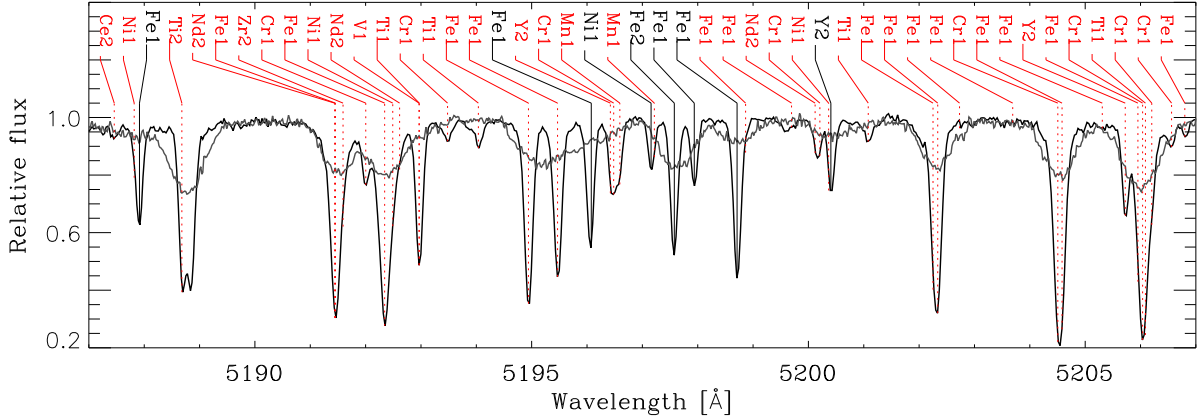
Fig. 4. Comparison of the spectra for the Sun and HD 110379 for which $v \sin i$ is 2 and 24 km s^{-1}. Atomic lines selected for abundance analysis of the Sun are marked with solid vertical lines, while the neighbouring spectral lines are marked with dotted lines.

from Grevesse & Sauval (1998). We are convinced that the analysis is still valid since it is carried out differentially with respect to an observed spectrum of the Sun. We have also did the analysis applying the new solar abundance for one of our reference stars, HD 110379, as an explicit check. The mean abundance is 0.02 dex higher using either Fe I and Fe II lines, which is certainly within the uncertainty on the metallicity. The derived values for the microturbulence, $T_{\rm eff}$, and $\log g$ are unchanged.

5. Parameters from photometry and parallaxes

5.1. Strömgren indices and 2MASS ($V - K$)

We have derived effective temperature ($T_{\rm eff}$), surface gravity ($\log g$), and metallicity ([Fe/H]) using both Strömgren indices and the $V - K$ colour from the 2MASS point source catalog (Cutri et al. 2003). Furthermore, we used parallaxes from HIPPARCOS to determine $\log g$. The fundamental atmospheric parameters of the sample of γ Dor stars we analysed are given in Table 1.

We used the TEMPLOGG software (Rogers 1995) to derive the fundamental atmospheric parameters from the Strömgren indices. The on-line version of TEMPLOGG provides uncertainty estimates that are too optimistic, since they are solely based on the uncertainties of the photometric indices. In Table 1 we quote uncertainties on $T_{\rm eff}$, $\log g$, and [Fe/H] of 250 K, 0.2 dex, and 0.1 dex (Rogers 1995; Kupka & Bruntt 2001).

We used Strömgren colour indices from the compilation of Hauck & Mermilliod (1998), but they were not available for two stars: HD 65526 and HD 218225. This H_{β} index was not available for HD 12901 and HD 14940 so interstellar reddening, $E(b - y)$, could not be determined. However, in all cases, $E(b - y) < 0.01$ with the exception of HD 125081, which has $E(b - y) = 0.045 \pm 0.005$. This star also has a high m_1 index, indicating the star is quite metal rich. From TEMPLOGG, we get [Fe/H] $= +0.54 \pm 0.10$, but this is based on an extrapolation from the calibration by Olsen (1988). The Strömgren indices for HD 110379 listed in SIMBAD are incorrect, as also noted by Scardia et al. (2007). Instead we used the average of the indices listed in Crawford et al. (1966), Cameron (1966), and Olsen (1983), which are all in good agreement. The Strömgren indices in Hauck & Mermilliod (1998) for HD 7455 are the mean of Stetson (1991) and Perry (1991), which are not in agreement:

the difference in the $b - y$ index is 0.086. Using the indices from Stetson (1991) yields $T_{\rm eff} = 5800$ K and $\log g = 4.9$, while Perry (1991) gives $T_{\rm eff} = 6460$ K and $\log g = 4.0$.

The $V - K$ colours from the 2MASS catalogue were used to estimate $T_{\rm eff}$ with the calibrations from Masana et al. (2006). We adopted the interstellar reddening from TEMPLOGG and assumed $E(b - y) = 0$ for the five stars where it was not available. We used $E(V - K) = 3.8\,E(b - y)$ using Cardelli et al. (1989). The $V - K$ calibration only has a weak dependence on [Fe/H] and $\log g$, so we assumed [Fe/H] $= -0.2 \pm 0.2$ and $\log g = 4.0 \pm 0.3$ for all stars. This is a valid assumption since the maximum change in $T_{\rm eff}$ is 40 K when changing either [Fe/H] or $\log g$ by $2\,\sigma$. The four brightest stars, HD 22001, HD 27290, HD 33262, and HD 110379, have $V < 5$, and their 2MASS K band magnitudes are based on saturated images. For this reason the errors are large, i.e. $\sigma_K = 0.23$ mag, instead of $\simeq 0.02$ mag for the other stars. For these stars the uncertainty on $T_{\rm eff}$ from the $V - K$ calibration is around 500 K, while for the other stars it is around 80–100 K. We find that $T_{\rm eff}$ from the Strömgren indices and $V - K$ agree within the uncertainties except for HD 110379. This star is part of the visual binary system γ Vir, and the companion, which has equal brightness, is within 4 arc seconds (Scardia et al. 2007).

5.2. $\log g$ from HIPPARCOS parallaxes

The Hertzsprung-Russell diagram for the stars is shown in Fig. 3. It is based on the adopted $T_{\rm eff}$ and luminosities calculated from the HIPPARCOS parallaxes and a solar bolometric magnitude of $M_{\rm bol,\odot} = 4.75$. In Fig. 3 we also show the γ Dor instability strip from Dupret et al. (2005) based on models with a mixing-length parameter $\alpha = 2.0$ along with evolution tracks from Lejeune & Schaerer (2001) for metallicities $Z = 0.008$ and $Z = 0.02$, which bracket the range for our targets. Each track is marked by the mass in solar units. From these tracks we can estimate the masses of the stars to be in the range 1.6–2.0 $M_{\odot}$. Since the target stars lie in the region of the "hook" of the evolution tracks, the uncertainty on the masses is $\simeq 0.2\,M_{\odot}$. We have assumed a common mass of $1.8 \pm 0.2\,M_{\odot}$ except for the well-studied binary star HD 110379, which has a known mass $M/M_{\odot} = 1.4$ (Scardia et al. 2007).

Table 2. Fundamental parameters obtained with VWA for the reference stars after perturbing the initial value of either $T_{\rm eff}$ or $\log g$.

Star	Pert.	$T_{\rm eff}$	$\log g$	[Fe/H]
Sun	p$T_{\rm eff}$	5760 ± 25	4.46 ± 0.03	-0.03 ± 0.05
	plog g	5780	4.51	-0.01
HD32115	p$T_{\rm eff}$	7630 ± 140	4.41 ± 0.09	$+0.10 \pm 0.11$
	plog g	7710	4.47	$+0.13$
HD37594	p$T_{\rm eff}$	7440 ± 160	4.18 ± 0.12	-0.26 ± 0.13
	plog g	7310	3.97	-0.33
HD49933	p$T_{\rm eff}$	6770 ± 90	4.24 ± 0.08	-0.43 ± 0.09
	plog g	6780	4.24	-0.42
HD110379	p$T_{\rm eff}$	7070 ± 130	4.03 ± 0.09	-0.04 ± 0.15
	plog g	7170	4.27	$+0.00$

Abbreviations used in second column:
p$T_{\rm eff}$= perturbation of $T_{\rm eff}$ = ± 300 K
plog g= perturbation of $\log g$ = ± 0.4 dex

We used this mass estimate, the adopted $T_{\rm eff}$, and the HIPPARCOS parallaxes to determine $\log g$ values. In particular we used[1] $\log g = 4[T_{\rm eff}] + [M] + 2\log \pi + 0.4(V + BC_V + 0.26) + 4.44$, where $[T_{\rm eff}] = \log(T_{\rm eff}/T_{\rm eff\odot})$ and $[M] = \log(M/M_\odot)$. We used bolometric corrections (BC_V) from the tables by Bessell et al. (1998). If we assume the mass is known to 10% and $T_{\rm eff}$ to 4% for all stars in the sample, the uncertainty on $\log g$ will depend on the uncertainty of the parallax: 13 out of 18 stars have uncertainties below 7%, while five stars, HD 7455, HD 26298, HD 125081, HD 126516, and HD 218225, have uncertainties around 15%. The uncertainty on $\log g$ is 0.13 dex and 0.20 dex for these two groups of stars. The $\log g$ values from the Strömgren c_1 index and the HIPPARCOS parallaxes agree, but the estimated uncertainty on the latter is significantly lower: typical uncertainties on $\log g$ are 0.2 and 0.1 dex, respectively.

6. Fundamental parameters from spectroscopy

Two important aims of the current work are to determine the fundamental parameters of the γ Dor stars and to compare their abundance pattern with other stars of similar spectral type. We first analyse a few stars with well-known parameters. We then analyse synthetic spectra in order to estimate uncertainties and make sure our method can be used to reliably constrain $T_{\rm eff}$, $\log g$, and metallicity. Based on these results we will decide on the approach for the detailed analysis of the target stars.

VWA can automatically adjust the microturbulence, $T_{\rm eff}$, and $\log g$ either simultaneously or any parameter can be fixed. This part of the analysis is based only on Fe lines, which are the most numerous in the stellar spectra. The iterative process of adjusting the parameters is to

– Minimize the correlation of Fe I abundance with equivalent width. This is done by adjusting the microturbulence.
– Minimize correlation between Fe I abundance and lower excitation potential of the atomic level causing the line. This is done by adjusting $T_{\rm eff}$.
– Minimize the difference in abundance of Fe I and Fe II lines. This is done by adjusting $\log g$.

Unfortunately, microturbulence and $T_{\rm eff}$ are not independent. Therefore, only the most sensitive lines are used to adjust the

[1] This expression is derived from the basic formulae $g \propto M/R^2$, $L \propto R^2 T_{\rm eff}^4$, and the definition of absolute magnitude, while assuming the solar values $M_{\rm bol} = 4.74$ and $\log g_\odot = 4.44$.

Table 3. Uncertainties on the fundamental parameters from the VWA analysis of synthetic spectra with two values of $T_{\rm eff}$ and with increasing $v \sin i$ for one value of $T_{\rm eff}$.

Model parameters		Uncertainties		
$v \sin i$ [km s^{-1}]	$T_{\rm eff}$ [K]	$\sigma(T_{\rm eff})$ [K]	$\sigma(\log g)$	$\sigma([{\rm Fe/H}])$
10	7250	40	0.03	0.02
10	6750	50	0.04	0.02
20	6750	110	0.08	0.03
40	6750	140	0.11	0.03
60	6750	200	0.13	0.04

microturbulence (typically EW < 80 mÅ), while we also use stronger lines (EW < 150 mÅ) to constrain $T_{\rm eff}$. For the slowly rotating stars, VWA needs to run 5–8 iterations before it converges. In each iteration, up to 120 lines are used and the CPU time is typically 1–3 hours for each star.

An important limitation to detailed spectroscopic analyses arises when the lines are broadened due to rotation. In Fig. 4 we show part of the spectrum for the CORALIE spectra of the Sun and the selected of lines for the abundance analysis. The spectrum of HD 110379, which has $v \sin i = 25$ km s^{-1}, is also shown for comparison. It is seen that line blending is worse, which illustrates that correct placement of the continuum can be difficult as $v \sin i$ increases. We will assess the importance of rotation by analysing synthetic spectra with increasing $v \sin i$ below.

6.1. Primary reference: solar spectrum from CORALIE

We used VWA to analyse a spectrum of the Sun measured with CORALIE. The S/N was 180, which is slightly higher than the spectra for the target stars. We ran the software with four models with parameters offset by ± 300 K in $T_{\rm eff}$ and ± 0.4 dex in $\log g$, respectively. In Table 2 we compare the results for the derived fundamental parameters. The results are very close to the canonical values of $T_{\rm eff} = 5777$ K, $\log g = 4.44$, and [Fe/H] = 0.00. The quoted uncertainties on $T_{\rm eff}$ and $\log g$ were estimated as is described in Sect. 7 and the quoted uncertainty on [Fe/H] is the *rms* value of the abundance determined from the Fe I lines. Uncertainties on $T_{\rm eff}$ are rounded off to 10 K. The uncertainties in Table 2 do not include any contribution from the uncertainty on the atmosphere models (cf. Sect. 3.1).

6.2. Secondary reference: the visual binary star HD 110379

HD 110379 is the A component in the visual binary system γ Vir, which has two identical components (Popper 1980). From the orbital mass, the HIPPARCOS parallax, and measured spectrophotometric fluxes, constraints can be placed on $\log g$ and $T_{\rm eff}$. Thus, Smalley et al. (2002) include HD 110379 in their sample of fundamental stars and derived $T_{\rm eff} = 7143 \pm 450$ K and $\log g = 4.21 \pm 0.02$.

We used HD 110379 to test the robustness of results from VWA. The S/N in the spectrum is 120, and the star has $v \sin i = 24$ km s^{-1} (part of the spectrum is shown in Fig. 4). For the initial model we used the $T_{\rm eff}$ and $\log g$ estimate from the Strömgren indices and the HIPPARCOS parallax, i.e. $T_{\rm eff} = 6860$ K and $\log g = 4.39$ (cf. Table 1). We also perturbed the initial guess for the fundamental parameters and converged at the parameters listed in Table 2. One of the results (plog g) is in excellent agreement with $\log g$ from the binary orbit, while the other result (p$T_{\rm eff}$) has lower values of both $T_{\rm eff}$ and $\log g$. This could be an indication that the determined values of $\log g$ and $T_{\rm eff}$ are

Table 4. The three groups of stars, depending on their $v \sin i$.

	Low $v \sin i$	Moderate	High
bf. γ Dor	167858	14940, 40745, 48501, 135825	12901, 27290, 65526, 218225
cand. γ Dor	110379, 126516		26298
bf. δ Scu	125081		
constant	7455, 22001, 33262		27604, 85964
reference	Sun (CORALIE), 32115, 37594, 49933		
Free param.	ξ_t, $T_{\rm eff}$, $\log g$	ξ_t, $T_{\rm eff}$	$T_{\rm eff}$

The first column is the variability type from De Cat et al. (2006).
The free parameters in the analysis are given below each group.

not independent, although the results for the tertiary reference stars, except perhaps for HD 37594, do not indicate that this is a general problem.

6.3. Tertiary references: HD 32115, HD 37594, HD 49933

We analysed CORALIE spectra of three slowly rotating A- and F-type stars for which detailed analyses have been published: HD 32115, HD 37594 (Bikmaev et al. 2002), and HD 49933 Gillon & Magain (2006). The fundamental parameters in these stars are constrained by photometric indices and spectroscopic analysis. Therefore, $\log g$ is known to about 0.15 dex from the parallax, which is about an order of magnitude worse than for the primary and secondary reference. The S/N in the three spectra from CORALIE is 200, 220, and 140 and the stars have $v \sin i$ = 9, 17, and 10 km s^{-1}.

As for the primary and secondary reference stars, we offset the initial parameters to test the convergence of VWA. The results are shown in Table 2. It is encouraging that for each star, the results agree within the error bars. The two slowly rotating A-type stars HD 32115 and HD 37594 were analysed by Bikmaev et al. (2002), who adopted a *fixed* value for $T_{\rm eff}$ based on Strömgren indices and the Hα line and $\log g$ from the HIPPARCOS parallax. The F-type star HD 49933 was analysed by Gillon & Magain (2006), who used an approach similar to VWA to fit $T_{\rm eff}$ and $\log g$ as part of the analysis.

Our results are in acceptable agreement with previous studies. The metallicities agree within 0.1 dex, while the largest difference in $T_{\rm eff}$ and $\log g$ are 200 K and 0.2. The differences are largest for HD 32115 and HD 37594, but we recall that $T_{\rm eff}$ and $\log g$ were not adjusted as part of the abundance analysis by Bikmaev et al. (2002). On the other hand, the agreement is good for HD 49933, in which case the VWA analysis is quite similar to the approach of Gillon & Magain (2006). We recall that we did not include NTLE effects, although for the two hottest stars, the effect on $\log g$ would be about +0.2 dex. However, the studies we are comparing with here also did not include any correction.

6.4. Abundance analysis of synthetic spectra

We tested VWA's ability to determine $T_{\rm eff}$, $\log g$, and metallicity by using synthetic spectra with the SYNTH code. This is the "ideal" case for abundance analysis since all $\log gf$ values are known and the spectrum is correctly normalized by design. Also, the input fundamental parameters are known. To mimic the quality of the observed data, we added random noise corresponding to S/N = 100 in the continuum. We calculated spectra with
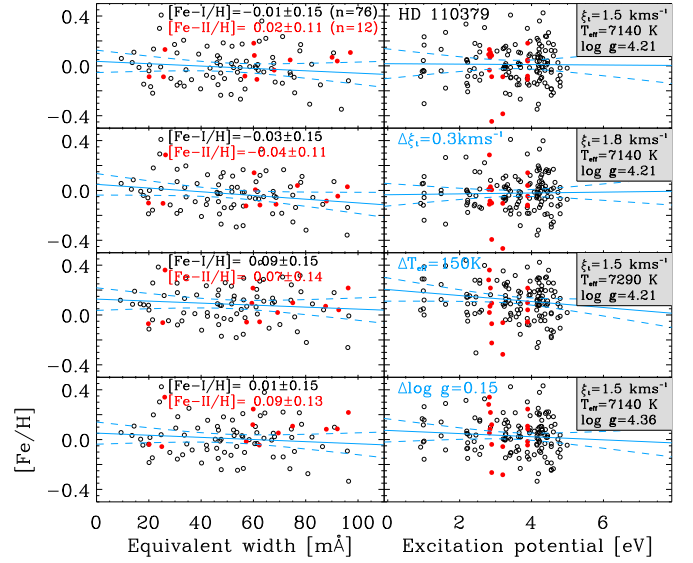

Fig. 5. Abundance of Fe in HD 110379 for four different atmosphere models. The *top panel* is for the adopted parameters, while the next three *panels* are for increased ξ_t, $T_{\rm eff}$, and $\log g$ (as indicated in the *right panels*). Fe I and Fe II lines are plotted with open and solid points, respectively. The solid line is a linear fit to the Fe I lines and the dashed lines indicate the 95% confidence limit of the fit.

$T_{\rm eff}$ = 6750 and 7250 K and $\log g$ = 4.3. For the cooler model, we used a range in $v \sin i$ of 10–60 km s^{-1}, and for the hotter one, we used $v \sin i$ = 10 km s^{-1}. The spectra were calculated in the range 4500–5600 Å where most of the lines are present. For slow rotation ($v \sin i < 20$), we used about 100 and 20 lines of Fe I and Fe II in the analysis. For the fast rotation (40 and 60 km s^{-1}), only half as many lines were used.

We offset the initial models in $T_{\rm eff}$ ($\pm$500 K) or $\log g$ (+0.4 dex) and let VWA determine the best parameters. For slow and moderate rotation, $v \sin i$ = 10–40 km s^{-1}, we found that the models converged satisfactorily: the largest difference in $T_{\rm eff}$, $\log g$, and [Fe/H] were 30 K, 0.05 dex, and 0.03 dex. For stars with high $v \sin i$ = 60 km s^{-1}, we found $\Delta T_{\rm eff}$ = 60 K, $\Delta \log g$ = 0.05, Δ[Fe/H] = 0.08.

We also calculated the uncertainties on $T_{\rm eff}$ and $\log g$ from the analysis of the synthetic spectra, and we list the results in Table 3. Uncertainties on the fundamental parameters from the models are not included (cf. Sect. 3.1). The last column gives the *rms* value of the Fe I and Fe II abundance. In comparison, the uncertainties for the observed secondary and tertiary reference stars listed in Table 2 are roughly twice as large. The reasons are likely a combination of imperfect continuum normalization, the remaining errors in the oscillator strengths, and differences in the temperature structure in the models and the real stars. The reference stars are all slowly rotating stars, but we may, as a first approximation, scale the uncertainties for the ideal case in Table 3 by a factor two. Thus, for stars with $v \sin i > 40$ km s^{-1}, the uncertainties become larger than the estimates from photometric indices or the HIPPARCOS parallax. We have therefore chosen not to use $T_{\rm eff}$ and $\log g$ as free parameters for stars with $v \sin i > 40$ km s^{-1}. We use this result when defining our strategy for the analysis of the target stars.

Table 5. Fundamental parameters determined with VWA for the 18 target stars and the four reference stars.

HD	T_{eff}	$\log g$	[M/H]	ξ_t [km s^{-1}]
7455	5840 ± 120	4.63 ± 0.14	−0.38 ± 0.08	1.0 ± 0.3
12901	6950 ± 220	F4.07 ± 0.13	−0.13 ± 0.16	F1.5 ± 0.4
14940	7380 ± 180	F4.25 ± 0.12	+0.01 ± 0.09	1.8 ± 0.3
22001	7010 ± 160	4.19 ± 0.14	−0.22 ± 0.08	2.6 ± 0.3
26298	6790 ± 200	3.95 ± 0.22	−0.27 ± 0.11	F1.5 ± 0.5
27290	7120 ± 200	F4.29 ± 0.18	+0.05 ± 0.14	F1.5 ± 0.5
27604	6320 ± 220	3.65 ± 0.24	+0.14 ± 0.08	F1.5 ± 0.5
33262	6440 ± 150	4.69 ± 0.16	−0.08 ± 0.09	1.3 ± 0.4
40745	6840 ± 180	F4.05 ± 0.12	−0.00 ± 0.09	1.7 ± 0.4
48501	7240 ± 190	F4.28 ± 0.12	+0.15 ± 0.11	1.5 ± 0.4
65526	7170 ± 210	F4.40 ± 0.13	−0.26 ± 0.13	F1.5 ± 0.5
85964	6600 ± 220	F4.14 ± 0.13	+0.11 ± 0.11	F1.5 ± 0.5
110379	7140 ± 160	F4.21 ± 0.02	−0.06 ± 0.09	1.5 ± 0.4
125081	6670 ± 140	3.02 ± 0.17	−0.29 ± 0.09	2.8 ± 0.4
126516	6590 ± 120	4.01 ± 0.15	−0.19 ± 0.08	1.9 ± 0.3
135825	7050 ± 180	F4.39 ± 0.13	+0.13 ± 0.09	1.5 ± 0.4
167858	7610 ± 150	4.35 ± 0.19	+0.22 ± 0.08	1.8 ± 0.3
218225	6920 ± 220	F4.31 ± 0.21	+0.57 ± 0.20	F1.5 ± 0.5
Sun	5770 ± 100	4.49 ± 0.10	−0.04 ± 0.08	0.6 ± 0.1
32115	7670 ± 170	4.44 ± 0.13	+0.08 ± 0.08	2.4 ± 0.2
37594	7380 ± 190	4.08 ± 0.16	−0.31 ± 0.08	2.5 ± 0.3
49933	6780 ± 130	4.24 ± 0.13	−0.46 ± 0.08	1.8 ± 0.2

Parameters marked by an *F* were held fixed in the analysis. Each uncertainty includes contributions from the model as described in the text. The $\log g$ value for HD 110379 is from Smalley et al. (2002).

6.5. Not all stars are equal: Low, moderate, and high $v \sin i$

Based on the analysis of the reference stars and the synthetic spectra, we have put the stars in three groups depending on their $v \sin i$ value in Table 4: low (4–25 km s^{-1}), moderate (35–40 km s^{-1}), and high $v \sin i$ (50–70 km s^{-1}). Furthermore, the stars are sorted according to the variability type from Paper I, i.e. either constant, candidate γ Dor, bona fide γ Dor, or bona fide δ Scuti stars.

The procedure for analysis with VWA depends on which group the star belongs to:

– For stars with low $v \sin i$, we allowed microturbulence, $\log g$ and T_{eff} as free parameters (seven stars).
– For stars with moderate rotation, we fixed $\log g$ from the HIPPARCOS parallaxes (the uncertainty is below 0.15 dex), but adjusted T_{eff} and microturbulence of the atmospheric models (four stars).
– For stars with a high rotation rate, there are not enough unblended lines to be able to constrain the microturbulence, $\log g$, and T_{eff}. We fixed the value of the microturbulence (= 1.5 km s^{-1}), used $\log g$ from the calibration using the HIPPARCOS parallax, and fitted only T_{eff} (seven stars).

7. Fundamental parameters

In Table 5 we list the final fundamental parameters of the 18 targets stars and the four reference stars. We list the average values from Table 2 for the reference stars. Note that for the moderate and fast rotators some of the parameters were held fixed and these are marked by F in Table 5, e.g. $\log g$ from the HIPPARCOS parallax.

Uncertainties on the fundamental parameters were estimated by evaluating the sensitivity to the changes in microturbulence,
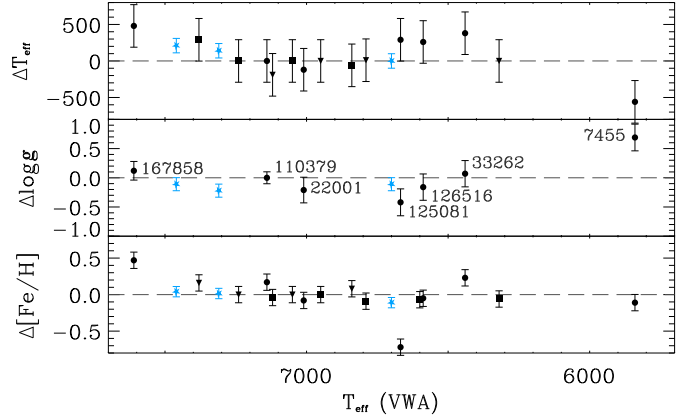
Fig. 6. Comparison of the fundamental parameters found from VWA and photometric indices. Circles, squares, and triangles are used for the slow, moderate, and fast rotators. Star symbols are used for the three tertiary reference stars. The HD numbers of the slow rotators are indicated in the *middle panel*.

T_{eff}, and $\log g$. In Fig. 5 we show examples for HD 110379. The *top panel* is for the final parameters and the following panels are for increased ξ_t, $\log g$, and T_{eff}, respectively. Following Gillon & Magain (2006), the uncertainty on T_{eff} is found by multiplying the change in T_{eff} by the ratio of the uncertainty of the slope and the change in slope, s, i.e. $\sigma(T_{\text{eff}}) = \Delta T_{\text{eff}} \cdot \sigma(s)/\Delta(s)$. This uncertainty is added quadratically to the estimated uncertainty from the model atmospheres as was discussed in Sect. 3.1.

The metallicity, [M/H], is computed as the average of the five metals Ca, Sc, Ti, Cr and Fe for both neutral and ionized lines, with the requirement that at least five lines were used for any element.

In Fig. 6 we show the differences between the parameters from VWA and the initial parameters (cf. Table 1). It is seen that some of the moderate and fast rotators have $\Delta T_{\text{eff}} = 0$ K because they are not very sensitive to changes in T_{eff}. For the slowly rotating stars, we find that in most cases T_{eff} and $\log g$ found by VWA is close to the initial model. A few exceptions are found that illustrate the importance of using more than one method to estimate the fundamental parameters.

The largest deviation is for HD 7455 where T_{eff} was 600 K lower and $\log g$ 0.7 dex higher than the initial model. Our result resolves the dispute over the discrepant Strömgren indices from the two different sources mentioned in Sect. 5.1. We find a large discrepancy for HD 125081, where we get a $\log g$ and metallicity that is 0.4 dex and 0.7 lower, respectively. This is the most evolved star and is also the only star with a significant interstellar reddening. If there was no interstellar reddening, [Fe/H] would be lower but not as low as we find from the abundance analysis. We find a high T_{eff} and high metallicity for HD 167858, but the uncertainty on T_{eff} is quite large.

8. Abundances

The abundances for the bona fide γ Dor and candidate γ Dor stars are shown in the *top panel* in Fig. 7, and results for the constant and reference stars are shown in the *bottom panel*. Results are only shown for the slow and moderate rotators. For each element, each point corresponds to the HD numbers in the same order from left to right in Tables A.1 and A.2. Note that the abundance of each element has been offset by the abundance of Fe I,
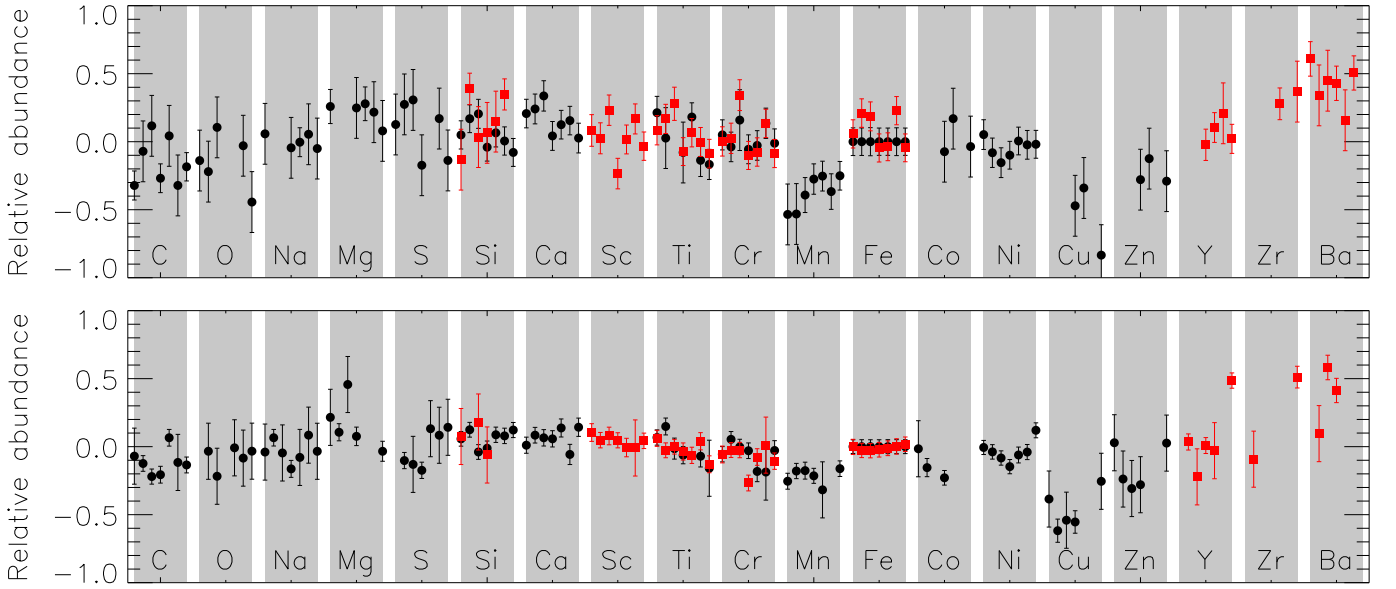
Fig. 7. Abundance pattern in the bona fide and three candidate γ Dor stars (*top panel*) and reference stars and constant stars (*bottom panel*). Only the results for slow and moderate rotators are shown. The abundances are plotted in the same order from left to right as the HD numbers in Tables A.1 and A.2. Note that the abundances are measured relative to the abundance of Fe I measured in each star.

which is our primary metallicity indicator. When this offset is applied we see the abundance pattern quite clearly, especially for the reference stars where nearly all abundances lie within 0.0 ± 0.2 dex. In Appendix A we list the individual abundances for all the stars we have analysed.

8.1. Abundance pattern in the constant stars

The *bottom panel* in Fig. 7 shows the results for the reference stars and the constant stars in the sample. We see systematic offsets of about −0.5 to +0.2 for C, Mn, Cu, Zn, and Ba, which to some extent may be explained by the assumption of LTE. However, for C the LTE correction for stars around 7000 K is *negative* and of the order of −0.1 dex (Rentzsch-Holm 1996). We included only the line transitions available in VALD, while for certain elements, like Ba (McWilliam 1998), hyperfine structure is important.

For the Fe-peak elements the scatter is quite low, while the scatter from star to star is higher for the lighter elements, C, O, Na, Mg, and S. For the light elements, C to S, typically 1–5 lines are available for each element (cf. Table A.2) and so the uncertainties are quite large due to any systematic errors due to erroneous continuum placement, blends, etc.

8.2. Abundance pattern in the γ Doradus stars

The *top panel* in Fig. 7 shows the abundance pattern for the bona fide γ Dor and candidate γ Dor stars. We see systematic offsets for C, Mn, Cu, Zr, and Ba, which is also seen for some elements in the reference and constant stars. For a given element we see that the scatter is larger than for the reference stars. However, four of the eight stars have moderate $v \sin i$, so fewer lines are available.

One of our goals of the present study is to find evidence of a link between chemical peculiarity and the γ Dor stars. In particular we searched for evidence of the following patterns:

- λ Boo: low abundance of Fe-peak elements, solar abundance of C, N, O, and S.
- Am: high abundance of Fe-peak elements, low abundance of Ca and Sc.

We do not find clear evidence of these patterns in any of the stars. It was noted by Handler (1999) that all γ Dor candidates have metallicities close to the solar value, based on the Strömgren m_1 index. This is supported by our detailed spectroscopic analyses, since [M/H] lies in the range −0.27 to +0.22 for 11 γ Dor candidates (see Table 5). The exception is the fast rotator HD 218225, but its value also has the largest uncertainty, [M/H] = 0.57±0.20.

8.3. Comparison with previous studies

Abundance studies have been done previously for three of the stars in our sample, HD 48501, HD 110379, and HD 167858. Boesgaard & Tripicco (1987) analysed HD 48501 and found [Fe/H] = +0.01 and [Ca/H] = +0.20, while we get [Fe/H] = −0.08 and [Ca/H] +0.23, which is in very good agreement. Our results also roughly agree with Boesgaard & Tripicco (1986), who found high metallicity in HD 167858 at [Fe/H] = +0.15 and [Ca/H] = +0.17, while we find [Fe/H] = +0.27 and [Ca/H] +0.32. These two studies were based on relatively few lines in a limited optical range. Erspamer & North (2003) analysed several elements in HD 110379, and we have good agreement with differences below 0.1 dex, although two elements, Mg and Sc, differ by 0.2 dex.

Detailed asteroseismic modelling was attempted for the bona fide γ Dor star HD 12901 by Moya et al. (2005). Their analysis was hampered by the uncertain metallicity of about [Fe/H] = −0.4 found from the Strömgren m_1 index. We find a metallicity of [M/H] = −0.13 ± 0.16, which we recommend using in future asteroseismic analyses of HD 12901. The star is a fast rotator with $v \sin i \simeq 64 \, \mathrm{km \, s^{-1}}$, so we cannot constrain T_{eff} and $\log g$ based on our analysis with VWA.

Two stars in our sample are included in the catalogue of Ap and Am stars compiled by Renson et al. (1991): HD 125081 is listed as a chemically peculiar star with abnormal abundances of Sr, Cr, and Eu. HD 167858 is noted as having a "doubtful nature", but the source of this claim is not given. Paunzen & Maitzen (1998) did not find any strong chemical peculiarity in these two stars based on their measurements of the Δp photometric index. Our present analyses of the stars support this result.

9. Conclusions

We have presented a detailed abundance analysis of a group of bona fide and candidate γ Dor stars. In addition we analysed a number of constant stars with similar stellar parameters. There seems to be larger scatter in the abundances for the γ Dor stars, but we find no strong evidence that the overall abundance pattern is different from other A- and F-type stars. Furthermore, the metallicity is quite close to the solar value in all cases. We have constrained the fundamental parameters of 18 single field stars from Paper I, of which about half are potential γ Dor stars.

We also analysed a few reference stars in order to thoroughly test the performance of the VWA software package. The software gives reliable results for the value of $T_{\rm eff}$ and $\log g$ for our primary and secondary reference stars, i.e. the Sun and the astrometric binary HD 110379; the latter has a well-determined $\log g$ but poorly determined $T_{\rm eff}$. Our results also agree well with previous analyses of three tertiary reference A- and F-type stars, although these single field stars do not have well-determined values of $T_{\rm eff}$ and $\log g$. Our analysis of synthetic spectra with increasing rotational velocity shows that, for stars with $v \sin i > 50\,{\rm km\,s^{-1}}$, our method cannot be used to constrain the microturbulence, $T_{\rm eff}$, and $\log g$ simultaneously. For the slowly rotating stars with $v \sin i < 25\,{\rm km\,s^{-1}}$, we can constrain $T_{\rm eff}$, $\log g$, and [Fe/H] to about 120 K, 0.13 dex, and 0.09 dex including estimated uncertainties of the applied model atmospheres. These results are certainly an improvement over photometric uncertainties, which are typically at least twice as large. We expect that our results will be useful in future astero-seismic studies of γ Dor stars.

References

Arentoft, T., de Ridder, J., Grundahl, F., et al. 2007, A&A, 465, 965
Balona, L. A., Krisciunas, K., & Cousins, A. W. J. 1994, MNRAS, 270, 905
Bessell, M. S., Castelli, F., & Plez, B. 1998, A&A, 333, 231
Bikmaev, I. F., Ryabchikova, T. A., Bruntt, H., et al. 2002, A&A, 389, 537
Boesgaard, A. M. & Tripicco, M. J. 1986, ApJ, 303, 724
Boesgaard, A. M. & Tripicco, M. J. 1987, ApJ, 313, 389
Breger, M., Lenz, P., Antoci, V., et al. 2005, A&A, 435, 955
Bruntt, H., Bikmaev, I. F., Catala, C., et al. 2004, A&A, 425, 683
Bruntt, H., Catala, C., Garrido, R., et al. 2002, A&A, 389, 345
Bruntt, H., Stello, D., Suárez, J. C., et al. 2007, MNRAS, 378, 1371
Cameron, R. C. 1966, Georgetown Observatory Monogram, 21, 0
Canuto, V. M. & Mazzitelli, I. 1992, ApJ, 389, 724
Cardelli, J. A., Clayton, G. C., & Mathis, J. S. 1989, ApJ, 345, 245
Crawford, D. L., Barnes, J. V., Faure, B. Q., & Golson, J. C. 1966, AJ, 71, 709
Cutri, R. M., Skrutskie, M. F., van Dyk, S., et al. 2003, 2MASS All Sky Catalog of point sources. (The IRSA 2MASS All-Sky Point Source Catalog, NASA/IPAC Infrared Science Archive. http://irsa.ipac.caltech.edu/applications/Gator/)
De Cat, P., Eyer, L., Cuypers, J., et al. 2006, A&A, 449, 281
Dupret, M.-A., Grigahcène, A., Garrido, R., et al. 2006, Memorie della Societa Astronomica Italiana, 77, 366
Dupret, M.-A., Grigahcène, A., Garrido, R., Gabriel, M., & Scuflaire, R. 2004, A&A, 414, L17
Dupret, M.-A., Grigahcène, A., Garrido, R., Gabriel, M., & Scuflaire, R. 2005, A&A, 435, 927
Erspamer, D. & North, P. 2003, A&A, 398, 1121
Gillon, M. & Magain, P. 2006, A&A, 448, 341
Gonzalez, G. 1998, A&A, 334, 221
Gray, R. O. & Kaye, A. B. 1999, AJ, 118, 2993
Grevesse, N., Asplund, M., & Sauval, A. J. 2007, Space Science Reviews, 105
Grevesse, N. & Sauval, A. J. 1998, Space Science Reviews, 85, 161
Handler, G. 1999, MNRAS, 309, L19
Hauck, B. & Mermilliod, M. 1998, A&AS, 129, 431
Heiter, U., Kupka, F., van't Veer-Menneret, C., et al. 2002, A&A, 392, 619
Henry, G. W. & Fekel, F. C. 2005, AJ, 129, 2026
Henry, G. W., Fekel, F. C., & Henry, S. M. 2007, AJ, 133, 1421
Hinkle, K., Wallace, L., Valenti, J., & Harmer, D. 2000, Visible and Near Infrared Atlas of the Arcturus Spectrum 3727–9300 Å (San Francisco: ASP)
King, H., Matthews, J. M., Rowe, J. F., et al. 2007, ArXiv e-prints, 706
Krisciunas, K. & Handler, G. 1995, Informational Bulletin on Variable Stars, 4195, 1
Kupka, F. 1996, in ASP Conf. Ser. 108: M.A.S.S., Model Atmospheres and Spectrum Synthesis, ed. S. J. Adelman, F. Kupka, & W. W. Weiss, 73
Kupka, F. & Bruntt, H. 2001, First COROT/MONS/MOST Ground Support Workshop, ed. C. Sterken (Vrije Universiteit Brussel, Belgium), 39
Kupka, F., Piskunov, N., Ryabchikova, T. A., Stempels, H. C., & Weiss, W. W. 1999, A&AS, 138, 119
Kurucz, R. 1993, SYNTHE Spectrum Synthesis Programs and Line Data. Kurucz CD-ROM No. 18. Cambridge, Mass.: Smithsonian Astrophysical Observatory
Lejeune, T. & Schaerer, D. 2001, A&A, 366, 538
Masana, E., Jordi, C., & Ribas, I. 2006, A&A, 450, 735
Mathias, P., Le Contel, J.-M., Chapellier, E., et al. 2004, A&A, 417, 189
McWilliam, A. 1998, AJ, 115, 1640
Moya, A., Suárez, J. C., Amado, P. J., Martin-Ruíz, S., & Garrido, R. 2005, A&A, 432, 189
Olsen, E. H. 1983, A&AS, 54, 55
Olsen, E. H. 1988, A&A, 189, 173
Paunzen, E. & Maitzen, H. M. 1998, A&AS, 133, 1
Perry, C. L. 1991, PASP, 103, 494
Popper, D. M. 1980, ARA&A, 18, 115
Renson, P., Gerbaldi, M., & Catalano, F. A. 1991, A&AS, 89, 429
Rentzsch-Holm, I. 1996, A&A, 312, 966
Rodríguez, E., Costa, V., Zhou, A.-Y., et al. 2006, A&A, 456, 261
Rogers, N. Y. 1995, Communications in Asteroseismology, 78, 1
Rowe, J. F., Matthews, J. M., Cameron, C., et al. 2006, Communications in Asteroseismology, 148, 34
Sadakane, K. 2006, PASJ, 58, 1023
Scardia, M., Argyle, R. W., Prieur, J.-L., et al. 2007, Astronomische Nachrichten, 328, 146
Smalley, B. 2005, Memorie della Societa Astronomica Italiana Supplement, 8, 130
Smalley, B., Gardiner, R. B., Kupka, F., & Bessell, M. S. 2002, A&A, 395, 601
Stetson, P. B. 1991, AJ, 102, 589
Suárez, J. C., Garrido, R., & Goupil, M. J. 2006a, A&A, 447, 649
Suárez, J. C., Goupil, M. J., & Morel, P. 2006b, A&A, 449, 673
Valenti, J. A. & Piskunov, N. 1996, A&AS, 118, 595
Zima, W., Wright, D., Bentley, J., et al. 2006, A&A, 455, 235

Appendix A: Detailed abundance results

In Tables A.1–A.3, we list the abundances of individual elements of the target stars. The abundances are measured differentially line-by-line with respect to an observed spectrum of the Sun published by Hinkle et al. (2000). The tables list the uncertainty on the mean value (in parenthesis) and the number of lines used in the analysis. For example, the abundance of Carbon in

HD 14940 is measured to be $\log N_\mathrm{C}/N_\mathrm{total} - (\log N_\mathrm{C}/N_\mathrm{total})_\odot =$ -0.38 ± 0.03 from four lines. The quoted uncertainty is an internal value and does not include contributions from the uncertainties on the adopted fundamental parameters or shortcomings of the applied model atmosphere, which contribute by about 0.08 dex on the uncertainty of the abundances (cf. Sect. 3.1).

Appendix B: Line list for HD 110379

In Table B.1 we list the lines used in the abundance analysis of HD 110379 with atomic parameters extracted from the VALD database (Kupka et al. 1999). It represents a typical example of lines used in the analysis for the slowly rotating stars in our sample.

Table A.1. Abundances for the bona fide and candidate γ Dor stars. The results are shown in the *top panel* in Fig. 7.

	HD 14940		HD 40745		HD 48501		HD 110379		HD 126516		HD 135825		HD 167858	
C I	−0.38(3)	4	−0.15	2	+0.04	1	−0.26(3)	5	−0.17(4)	3	−0.30	1	+0.08(2)	7
O I	−0.19	1	−0.30	1	+0.03	1	–	–	–	–	−0.01	1	−0.17	2
Na I	+0.00	2	–	–	–	–	−0.02	2	−0.21(3)	5	+0.07	2	+0.23(4)	3
Mg I	+0.20(7)	5	–	–	–	–	+0.27(7)	3	+0.07(7)	4	+0.23(7)	3	+0.35	2
S I	+0.07	2	+0.20	1	+0.23	1	−0.15(3)	3	–	–	+0.19	2	+0.14	2
Si I	−0.01(2)	10	+0.09(2)	16	+0.13(3)	6	−0.02(2)	15	−0.14(2)	8	+0.02(2)	12	+0.20(2)	11
Si II	−0.19(6)	3	+0.31(5)	4	−0.04(5)	3	+0.09	2	−0.06	1	+0.36(5)	4	–	–
Ca I	+0.15(3)	20	+0.16(4)	14	+0.26(4)	9	+0.06(3)	17	−0.08(3)	14	+0.17(3)	20	+0.30(4)	7
Sc II	+0.03(5)	4	−0.05(5)	4	+0.16(4)	4	−0.21(5)	7	−0.19(3)	8	+0.18(4)	6	+0.24(2)	7
Ti I	+0.16(6)	4	−0.05	2	–	–	−0.06	2	−0.07(3)	14	−0.12(6)	4	+0.11(4)	5
Ti II	+0.04(3)	10	+0.09(3)	11	+0.20(6)	6	−0.10(2)	33	−0.17(2)	12	+0.01(3)	12	+0.18(3)	7
Cr I	−0.01(4)	9	−0.11(4)	9	+0.08(6)	3	−0.04(3)	14	−0.24(4)	9	+0.15(4)	10	+0.26(3)	9
Cr II	−0.05(3)	7	−0.05(4)	7	+0.27(5)	5	−0.08(2)	17	−0.28(2)	9	+0.15(2)	13	+0.19(2)	9
Mn I	−0.59	2	−0.61	2	−0.47(8)	4	−0.25(4)	8	−0.46(4)	10	−0.35(8)	4	+0.03(3)	11
Mn II	–	–	–	–	–	–	–	–	–	–	–	–	–	–
Fe I	−0.06(1)	42	−0.08(1)	89	−0.08(2)	20	+0.02(0)	146	−0.21(1)	133	+0.01(2)	41	+0.27(1)	83
Fe II	+0.00(2)	13	+0.13(3)	12	+0.11(3)	8	−0.03(2)	17	−0.25(2)	19	+0.25(2)	13	+0.23(2)	12
Co I	–	–	–	–	–	–	−0.05	1	−0.04	2	–	–	+0.24	1
Ni I	−0.00(4)	8	−0.16(4)	9	−0.23(4)	7	−0.08(2)	27	−0.20(1)	29	−0.01(3)	12	+0.26(2)	16
Cu I	–	–	–	–	–	–	−0.45	2	−0.55	2	–	–	−0.56	1
Zn I	–	–	–	–	–	–	−0.26(7)	3	−0.33(5)	3	–	–	−0.01	2
Y I	–	–	–	–	–	–	–	–	–	–	–	–	–	–
Y II	–	–	–	–	–	–	−0.01(5)	4	−0.11(4)	7	+0.23	2	+0.30(3)	4
Zr II	–	–	–	–	–	–	–	–	+0.05(6)	4	–	–	+0.64	1
Ba II	+0.56(7)	4	+0.26	2	+0.37	2	+0.46(7)	5	−0.05(10)	3	+0.54(7)	4	–	–

Table A.2. Abundances for the constant stars, the bona fide δ Scuti star HD 125081, and the tertiary reference stars (HD 32115, HD37594, and HD 49933). The results are shown in the *bottom panel* in Fig. 7.

	HD 7455		HD 22001		HD 32115		HD 33262		HD 37594		HD 49933		HD 125081	
C I	−0.45	2	−0.38(2)	6	−0.15(2)	9	−0.25(3)	4	−0.24(3)	4	−0.56(4)	3	−0.41(3)	6
O I	–	–	−0.29	2	−0.15	2	–	–	−0.32	2	−0.53	2	−0.31	2
Na I	−0.42	2	−0.19(3)	7	+0.03	2	−0.21(3)	6	−0.39	2	−0.36	2	−0.31	2
Mg I	−0.16(7)	3	−0.15(3)	7	+0.53(9)	3	+0.03(4)	7	–	–	–	–	−0.31(5)	4
S I	–	–	−0.36(3)	4	−0.06(3)	3	−0.22(3)	5	−0.18	1	−0.36	1	−0.14(3)	3
Si I	−0.32(1)	14	−0.13(2)	12	+0.03(2)	15	−0.06(1)	18	−0.22(2)	9	−0.37(2)	8	−0.16(2)	11
Si II	−0.31	2	–	–	+0.25	2	−0.11	2	–	–	–	–	–	–
Ca I	−0.37(3)	15	−0.17(2)	16	+0.14(3)	15	+0.01(3)	11	−0.17(4)	8	−0.50(5)	5	−0.14(4)	8
Sc II	−0.28(4)	4	−0.21(2)	11	+0.15(4)	6	+0.00(2)	14	−0.32(4)	4	−0.45(4)	3	−0.24(2)	12
Ti I	−0.31(2)	16	−0.11(3)	9	+0.06(5)	5	−0.11(3)	7	–	–	−0.52(6)	4	−0.44	2
Ti II	−0.32(3)	10	−0.28(2)	19	+0.07(2)	29	−0.08(3)	5	−0.37(3)	7	−0.41(3)	4	−0.41(3)	7
Cr I	−0.44(2)	19	−0.20(2)	14	+0.07(2)	20	−0.07(2)	13	−0.49(5)	4	−0.63(7)	3	−0.31(5)	5
Cr II	−0.44(3)	6	−0.28(2)	15	+0.05(2)	12	−0.31(2)	7	−0.39(3)	6	−0.43(4)	3	−0.38(3)	8
Mn I	−0.63(3)	12	−0.43(2)	19	−0.10(3)	10	−0.26(2)	22	−0.63	2	–	–	−0.44(2)	15
Fe I	−0.38(0)	226	−0.26(0)	108	+0.07(0)	189	−0.04(0)	103	−0.31(1)	82	−0.44(1)	86	−0.28(1)	98
Fe II	−0.38(2)	16	−0.29(1)	28	+0.04(1)	32	−0.07(2)	21	−0.32(2)	17	−0.44(2)	12	−0.26(1)	22
Co I	−0.40(4)	3	−0.41(4)	5	–	–	−0.27(1)	16	–	–	–	–	–	–
Ni I	−0.39(1)	45	−0.29(1)	29	−0.01(1)	33	−0.19(1)	32	−0.37(2)	11	−0.48(2)	14	−0.16(2)	17
Cu I	−0.77	2	−0.87(6)	4	−0.47	2	−0.60(6)	4	–	–	–	–	−0.53(7)	3
Zn I	−0.35	2	−0.49(6)	3	−0.24	2	−0.32(6)	3	–	–	–	–	−0.25(6)	3
Y II	–	–	−0.22(3)	8	−0.15(5)	3	−0.04(3)	8	−0.34(4)	3	–	–	+0.21(2)	8
Zr II	–	–	−0.35	2	–	–	–	–	–	–	–	–	+0.23(6)	4
Ba II	–	–	−0.16	2	+0.65(7)	5	+0.37(7)	4	–	–	–	–	+0.80(11)	4

Table A.3. Abundances in the target stars with high $v \sin i$.

	HD 12901		HD 26298		HD 27290		HD 27604		HD 65526		HD 85964		HD 218225	
C I	+0.26(3)	3	−0.47	2	+0.10(4)	4	−	−	−	−	−0.05	2	−	−
O I	−	−	−	−	+0.14	1	−	−	−	−	−	−	−	−
Na I	−0.29	2	−	−	−0.88(7)	3	−	−	−	−	−	−	−	−
Mg I	−0.07	2	+0.07	2	−	−	−	−	−	−	−	−	−	−
S I	−0.13	2	−0.14	2	+0.19(3)	3	−	−	−0.02	1	+0.47	2	−	−
Si I	−0.40(3)	7	−0.03(3)	4	+0.06(2)	12	+0.54(6)	3	−0.25	2	+0.07(3)	6	−	−
Si II	+0.15	2	−0.00	2	+0.63	2	−	−	+0.15	2	−	−	−	−
Ca I	+0.09(4)	10	+0.02(4)	11	+0.29(3)	15	+0.16(7)	5	−	−	+0.34(5)	8	+0.81(5)	8
Sc II	−	−	−0.43(7)	3	−	−	−	−	−	−	+0.14(7)	3	−	−
Ti I	−	−	−	−	+0.19	2	−	−	−	−	−	−	−	−
Ti II	−0.49(5)	4	−0.38(6)	5	−0.38(3)	9	+0.16	2	−	−	+0.01(4)	8	+0.65(7)	4
Cr I	−0.60(6)	4	−0.27	2	−0.07(4)	6	−	−	−	−	−0.24(6)	4	−0.22(7)	3
Cr II	−0.34	2	−0.38(4)	5	+0.00(3)	10	−	−	−	−	−0.01(4)	7	−	−
Mn I	−	−	−	−	−0.18(8)	4	+0.19	2	−	−	−	−	−	−
Mn II	−	−	−	−	−	−	−	−	−	−	−	−	−	−
Fe I	−0.24(1)	75	−0.30(1)	75	+0.12(1)	117	+0.13(1)	73	−0.33(2)	41	+0.10(1)	56	+0.29(1)	61
Fe II	−0.24(4)	8	−0.29(2)	15	+0.32(2)	17	+0.13(3)	9	−0.19(4)	5	+0.12(3)	14	+0.62(3)	10
Ni I	+0.13(5)	5	−0.32(5)	6	+0.12(4)	10	−	−	−0.37(7)	3	−0.03(5)	6	−	−
Zn I	−	−	−	−	−	−	−	−	−	−	−	−	−	−
Y I	−	−	−	−	−	−	−	−	−	−	−	−	−	−
Zr II	−	−	−	−	−	−	−	−	−	−	−	−	−	−
Ba II	+0.35	2	−	−	+0.56	2	−	−	−	−	−	−	−	−

Table B.1. The atomic number, element name, wavelength, and log gf from the VALD database for the lines used in the analysis of HD 110379.

El.	λ [Å]	log gf	El.	λ [Å]	log gf	El.	λ [Å]	log gf	El.	λ [Å]	log gf	El.	λ [Å]	log gf
^{6}C I	4770.026	−2.439	Ti I	5210.385	−0.884	Fe I	4757.582	−2.321	Fe I	5434.524	−2.122	Fe I	6408.018	−1.018
C I	4932.049	−1.884	Ti II	4501.273	−0.760	Fe I	4791.246	−2.435	Fe I	5441.339	−1.730	Fe I	6419.950	−0.240
C I	5380.337	−1.842	Ti II	4518.327	−2.640	Fe I	4802.880	−1.514	Fe I	5445.042	−0.020	Fe I	6421.351	−2.027
C I	6587.610	−1.596	Ti II	4544.028	−2.530	Fe I	4843.144	−1.840	Fe I	5466.396	−0.630	Fe I	6609.110	−2.692
^{8}O I	6158.186	−0.409	Ti II	4563.761	−0.790	Fe I	4909.384	−1.273	Fe I	5472.709	−1.495	Fe I	6677.987	−1.418
^{11}Na I	5688.205	−0.450	Ti II	4589.958	−1.620	Fe I	4942.459	−1.409	Fe I	5473.900	−0.760	Fe I	6750.153	−2.621
^{12}Mg I	4702.991	−0.666	Ti II	4779.985	−1.260	Fe I	4946.388	−1.170	Fe I	5483.099	−1.407	Fe I	6810.263	−0.986
Mg I	5172.684	−0.402	Ti II	4805.085	−0.960	Fe I	4966.089	−0.871	Fe I	5497.516	−2.849	Fe II	4520.224	−2.600
Mg I	5183.604	−0.180	Ti II	5010.212	−1.300	Fe I	4967.890	−0.622	Fe I	5501.465	−3.047	Fe II	4541.524	−2.790
Mg I	5528.405	−0.620	Ti II	5013.677	−1.990	Fe I	4969.918	−0.710	Fe I	5506.779	−2.797	Fe II	4576.340	−2.920
Mg I	5711.088	−1.833	Ti II	5129.152	−1.300	Fe I	4973.102	−0.950	Fe I	5543.150	−1.570	Fe II	4620.521	−3.240
^{13}Al I	6696.023	−1.347	Ti II	5211.536	−1.356	Fe I	4988.950	−0.890	Fe I	5560.212	−1.190	Fe II	4731.453	−3.000
Al I	6698.673	−1.647	Ti II	5381.015	−1.970	Fe I	4994.130	−3.080	Fe I	5563.600	−0.990	Fe II	5120.352	−4.214
^{14}Si I	5645.613	−2.140	Ti II	5490.690	−2.650	Fe I	5014.943	−0.303	Fe I	5569.618	−0.486	Fe II	5256.938	−4.250
Si I	5675.417	−1.030	Ti II	6491.561	−1.793	Fe I	5027.120	−0.559	Fe I	5576.089	−1.000	Fe II	5362.869	−2.739
Si I	5708.400	−1.470	^{24}Cr I	4626.174	−1.320	Fe I	5028.126	−1.123	Fe I	5586.756	−0.120	Fe II	6084.111	−3.780
Si I	5747.667	−0.780	Cr I	4646.148	−0.700	Fe I	5029.618	−2.050	Fe I	5633.947	−0.270	Fe II	6147.741	−2.721
Si I	5753.623	−0.830	Cr I	4718.426	+0.090	Fe I	5054.643	−1.921	Fe I	5638.262	−0.870	Fe II	6149.258	−2.720
Si I	6125.021	−0.930	Cr I	5204.506	−0.208	Fe I	5067.150	−0.970	Fe I	5686.530	−0.446	Fe II	6238.392	−2.630
Si I	6131.852	−1.140	Cr I	5206.038	+0.019	Fe I	5074.748	−0.200	Fe I	5701.545	−2.216	Fe II	6247.557	−2.310
Si I	6145.016	−0.820	Cr I	5208.419	+0.158	Fe I	5076.262	−0.767	Fe I	5705.992	−0.530	Fe II	6416.919	−2.650
Si I	6194.416	−1.900	Cr I	5296.691	−1.400	Fe I	5090.774	−0.400	Fe I	5717.833	−1.130	Fe II	6432.680	−3.520
Si I	6237.319	−0.530	Cr I	5297.376	+0.167	Fe I	5121.639	−0.810	Fe I	5731.762	−1.300	^{27}Co I	5342.695	+0.690
Si I	6243.815	−0.770	Cr I	5348.312	−1.290	Fe I	5123.720	−3.068	Fe I	5752.023	−1.267	^{28}Ni I	4715.757	−0.320
Si I	6244.466	−0.690	Cr I	5787.965	−0.083	Fe I	5131.469	−2.515	Fe I	5762.992	−0.450	Ni I	4756.510	−0.270
Si I	6254.188	−0.600	Cr II	4554.988	−1.282	Fe I	5133.689	+0.140	Fe I	5809.218	−1.840	Ni I	4829.016	−0.330
Si I	6414.980	−1.100	Cr II	4558.650	−0.449	Fe I	5141.739	−1.964	Fe I	5816.373	−0.601	Ni I	4904.407	−0.170
Si II	6347.109	+0.297	Cr II	4588.199	−0.627	Fe I	5150.840	−3.003	Fe I	5859.578	−0.398	Ni I	4935.831	−0.350
Si II	6371.371	−0.003	Cr II	4634.070	−0.990	Fe I	5151.911	−3.322	Fe I	5862.353	−0.058	Ni I	4937.341	−0.390
^{16}S I	6046.027	−1.030	Cr II	4824.127	−0.970	Fe I	5159.058	−0.820	Fe I	5883.817	−1.360	Ni I	4980.166	+0.070
S I	6052.674	−0.740	Cr II	5237.329	−1.160	Fe I	5162.273	+0.020	Fe I	5930.180	−0.230	Ni I	4998.218	−0.690
S I	6757.171	−0.310	Cr II	5274.964	−1.290	Fe I	5194.942	−2.090	Fe I	5934.655	−1.170	Ni I	5081.107	+0.300
^{20}Ca I	4878.126	+0.430	Cr II	5305.853	−2.357	Fe I	5198.711	−2.135	Fe I	5987.066	−0.556	Ni I	5082.339	−0.540
Ca I	5349.465	−1.178	Cr II	5308.408	−1.846	Fe I	5217.389	−1.070	Fe I	6003.012	−1.120	Ni I	5084.089	+0.030
Ca I	5581.965	−0.569	Cr II	5310.687	−2.280	Fe I	5228.377	−1.290	Fe I	6008.554	−1.078	Ni I	5155.762	+0.011
Ca I	5588.749	+0.313	Cr II	5313.563	−1.650	Fe I	5242.491	−0.967	Fe I	6020.169	−0.270	Ni I	5663.975	−0.430
Ca I	5590.114	−0.596	Cr II	5334.869	−1.562	Fe I	5243.777	−1.150	Fe I	6024.058	−0.120	Ni I	5694.977	−0.610
Ca I	5594.462	+0.051	Cr II	5508.606	−2.110	Fe I	5250.646	−2.181	Fe I	6027.051	−1.089	Ni I	5715.066	−0.352
Ca I	5598.480	−0.134	^{25}Mn I	4754.042	−0.086	Fe I	5253.462	−1.573	Fe I	6056.005	−0.460	Ni I	5760.828	−0.800
Ca I	5857.451	+0.257	Mn I	4761.512	−0.138	Fe I	5281.790	−0.834	Fe I	6065.482	−1.530	Ni I	5805.213	−0.640
Ca I	6122.217	−0.386	Mn I	4762.367	+0.425	Fe I	5302.302	−0.720	Fe I	6078.491	−0.424	Ni I	6086.276	−0.530
Ca I	6162.173	−0.167	Mn I	4783.427	+0.042	Fe I	5315.070	−1.550	Fe I	6127.907	−1.399	Ni I	6116.174	−0.677
Ca I	6163.755	−1.303	Mn I	4823.524	+0.144	Fe I	5339.929	−0.647	Fe I	6136.615	−1.400	Ni I	6176.807	−0.260
Ca I	6166.439	−1.156	Mn I	5377.637	−0.109	Fe I	5341.024	−1.953	Fe I	6170.507	−0.440	Ni I	6767.768	−2.170
Ca I	6169.042	−0.804	Mn I	6021.819	+0.034	Fe I	5361.625	−1.430	Fe I	6173.336	−2.880	^{29}Cu I	5105.537	−1.516
Ca I	6169.563	−0.527	^{26}Fe I	4547.847	−1.012	Fe I	5364.871	+0.228	Fe I	6213.430	−2.482	Cu I	5782.127	−1.720
Ca I	6439.075	+0.394	Fe I	4566.989	−2.080	Fe I	5373.709	−0.860	Fe I	6219.281	−2.433	^{30}Zn I	4680.134	−0.815
Ca I	6449.808	−1.015	Fe I	4602.941	−2.209	Fe I	5379.574	−1.514	Fe I	6230.723	−1.281	Zn I	4722.153	−0.338
Ca I	6493.781	+0.019	Fe I	4607.647	−1.545	Fe I	5389.479	−0.410	Fe I	6232.641	−1.223	Zn I	4810.528	−0.137
Ca I	6499.650	−0.719	Fe I	4613.203	−1.670	Fe I	5391.461	−0.825	Fe I	6252.555	−1.687	^{39}Y II	4900.120	−0.090
Ca I	6717.681	−0.596	Fe I	4625.045	−1.340	Fe I	5393.168	−0.715	Fe I	6256.361	−2.408	Y II	5087.416	−0.170
^{21}Sc II	4670.407	−0.576	Fe I	4632.912	−2.913	Fe I	5398.279	−0.670	Fe I	6265.134	−2.550	Y II	5200.406	−0.570
Sc II	5031.021	−0.400	Fe I	4638.010	−1.119	Fe I	5400.502	−0.160	Fe I	6270.225	−2.464	^{40}Zr II	5112.297	−0.590
Sc II	5239.813	−0.765	Fe I	4733.592	−2.988	Fe I	5405.775	−1.844	Fe I	6335.331	−2.177	^{56}Ba II	4934.076	−0.150
Sc II	5684.202	−1.074	Fe I	4735.844	−1.325	Fe I	5410.910	+0.398	Fe I	6336.824	−0.856	Ba II	5853.668	−1.000
Sc II	6604.601	−1.309	Fe I	4736.773	−0.752	Fe I	5415.199	+0.642	Fe I	6338.877	−1.060	Ba II	6141.713	−0.076
^{22}Ti I	4981.731	+0.504	Fe I	4745.800	−1.270	Fe I	5424.068	+0.520	Fe I	6380.743	−1.376	Ba II	6496.897	−0.377